Published as: Katalee Jariyavidyanont, Walter Focke & René Androsch. Crystallization kinetics of polyamide 11 in the presence of sepiolite and montmorillonite nanofillers. Colloid Polym Sci (2016) 294:1143–1151. DOI 10.1007/s00396-016-3874-y

Crystallization kinetics of polyamide 11 in presence of sepiolite and montmorillonite nanofillers

Katalee Jariyavidyanont[a], Bindu Patanair[b], Walter Focke[b], and René Androsch[a*]

[a] Center of Engineering Sciences, Martin Luther University Halle-Wittenberg, 06099 Halle/Saale, Germany

[b] University of Pretoria, Institute of Applied Materials, Department of Chemical Engineering, Private Bag X20, Hatfield 0028, Pretoria, South Africa

Abstract

The crystallization kinetics of polyamide 11 (PA 11) in presence of sepiolite and organo-modified montmorillonite nanofillers has been studied in a wide range of temperatures and cooling rates by conventional differential scanning calorimetry (DSC) and fast scanning chip calorimetry (FSC). The presence of the nanofillers has a negligible effect on the crystallization temperature of PA 11 at low cooling rates. However, at rapid cooling conditions a distinct nucleating effect of the nanofillers is detected. The critical cooling rate to suppress crystallization increases from 600 K s^{-1} to about 1000 and 3000 K s^{-1} in nanocomposites containing sepiolite and montmorillonite, respectively. Regardless the cooling rate applied for solidification the melt, in the nanocomposites the crystallinity of PA 11 is 5 to 10 % higher than in neat PA 11, with the highest values obtained for the montmorillonite-containing system. The nucleating effect of the nanofillers onto the crystallization of the PA 11 is confirmed by analysis of the half-times of isothermal crystallization, and by analysis of the spherulitic superstructure. All measurements proved a saturation of the nucleation efficiency at a loading of the nanofiller of 2.5 m%.

Keywords: Polyamide 11, Nanocomposite, Crystallization, Fast scanning chip calorimetry

* Corresponding author:
E-mail: rene.androsch@iw.uni-halle.de
Phone: +49 3461 46 3762

Introduction

Polyamide 11 (PA 11) is a bio-based crystallizable polymer which is produced from renewable castor oil. It is gaining increasing importance due to its potential to replace petroleum based polymers. It is used for many high-performance engineering applications due to its balanced property profile including relatively high thermal stability, excellent chemical resistance, and reasonable mechanical characteristics [1]. As a rule, holding for all crystallizable polymers [2], the properties of PA 11 depend on the semicrystalline morphology which can be adjusted in wide ranges regarding the structure, fraction, shape and spatial arrangement of crystals. Major tools to control such structural parameters are the variation of the condition of melt-crystallization [3], or the addition of nucleating agents, promoting the crystallization process [4]. Though typically added to tailor properties according to composite rules [5], in this work the effect of presence of two different types of nanofillers on the crystallization kinetics and the semi-crystalline morphological structure of PA 11 is evaluated.

Regarding the crystallization behavior of unmodified PA 11 it is known that, depending on the crystallization conditions, different crystal structures may form [6–11]. Slow cooling of the melt leads to formation of triclinic δ-crystals which convert reversibly to α-crystals at the Brill-transition temperature [12] of about 100 °C. The equilibrium melting temperature of the α-structure is between 203 and 220 °C [13, 14] and the bulk enthalpy of fusion is between 189 and 244 J g^{-1} [13–15]. These crystals, which form at low supercooling of the melt, are of lamellar shape and are organized within spherulites [16]. Rapid cooling of the melt at rates between 100 and 500 K s^{-1} suppresses δ/α-crystal formation at low supercooling and leads to development of a pseudohexagonal δ'-phase of nodular shape at temperatures lower than 80 °C [3, 9]; even faster cooling prevents all ordering and causes complete vitrification of the melt at the glass transition temperature T_g of around 40 °C [3]. Recent analysis of the rate of isothermal crystallization revealed maxima at about 105 and 70 °C [3], with the bimodal dependence of the crystallization rate on temperature related to the occurrence of different nucleation mechanisms; this view is supported by an analysis of the nucleation density of samples crystallized at different supercooling [17].

For many polymers including polypropylene [18–20], polyoxymethylene [21], poly(ethylene terephthalate) [22], poly(butylene terephthalate) [23], poly(butene-1) [24], but in particular polyamides [25–34], it has been shown that addition of nanofillers often

enhance crystallization and even support the formation of specific crystal polymorphs. In fewer cases, however, a retardation of the crystallization process has also been reported, likely due to an immobilization of polymer chain segments at the polymer/nanofiller interface [35, 36].

Crystallization studies on nanocomposites based on PA 11 included analysis of half-times of crystallization and of the cooling-rate dependence of the crystallization temperature [37], and analysis of the X-ray structure of injection-molded test bars [38] or as-extruded pellets [39]. Half-times of crystallization were measured at rather low supercooling of the melt providing information that presence of montmorillonite (MMT) nanofiller is connected with an acceleration of the crystallization process. In addition it was found that the crystallization temperature of PA 11 on cooling the melt at rates between 2.5 and 20 K min^{-1} was increased. In a further study of PA 11/MMT nanocomposites for use in angioplasty balloon applications it was found that addition of MMT into PA 11 led to a distinct decrease of the half-time of isothermal crystallization. However, the accelerating effect of the nanofiller on the crystallization of PA 11 faded at loadings exceeding 2 m% [40]. Only recently the research of the crystallization behavior of PA 11 in presence of nanofillers has been expanded towards the application conditions relevant in polymer processing, that is, to analysis of the crystallization at rapid-cooling conditions and at high supercooling of the melt [41]. It was found for a specific system containing 5 m% organo-modified MMT (OMMT) that the PA 11 crystallization temperature was only increased on cooling faster than about 1 K s^{-1} and that the critical cooling rate to suppress crystallization of PA 11 was significantly increased. Similar observations have been reported for nanocomposites based on PA 6 [32].

In the present work, the prior research of the effect of nanofillers on the crystallization of PA 11 is expanded such to compare the nucleation efficiency of layer-like organo-modified montmorillonite (OMMT) and needle-like sepiolite, added at different concentrations into PA 11. These two nanofillers exhibit largely different shape/aspect ratio, and surface chemistry and it has been shown for nanocomposites based on PA 6 that, for these reasons, sepiolite has a higher reinforcing efficiency than MMT [42, 43]. Similar observations were obtained in studies of properties of nanocomposites based on poly(lactic acid) and poly(ε-caprolactone) [44]. To the best of our knowledge, research about crystallization of PA 11 in presence of sepiolite nanofillers has not yet been performed. In this study, therefore,

crystallization experiments are presented, with the purpose to compare the nucleating effect of sepiolite and OMMT nanofillers on the crystallization of PA 11. In advance to the numerous prior crystallization studies on polymer based nanocomposites, we employed in addition to conventional differential scanning calorimetry (DSC) a fast scanning chip calorimeter (FSC), allowing cooling the melt at rates up to several thousand K s^{-1} and to gain therefore novel information about structure formation of PA 11 based nanocomposites at processing relevant conditions.

Experimental

Materials and preparation

In this study a high-viscosity, natural PA 11 extrusion grade Rilsan BESNO TL from Atofina with a melting volume index of 1 cm^3 $(10\ min)^{-1}$ (235 °C, 2.16 kp) was used [1]. Needle-like sepiolite Pangel S9 (Tolsa, Spain) and layer-like organo-modified montmorillonite Cloisite 30B (Southern Clay, USA) were employed as nanofillers. The nanocomposites were prepared by a melt-compounding using a Nanjing Ouli Extrusion Machinery Co., Ltd. model TE-30/600-11-40 co-rotating twin-screw extruder (screw diameter = 30 mm, L/D = 40). The compounding was carried out with barrel temperature of 200 °C and a screw speed of 202 rpm. Before extrusion, the nanofillers and PA 11 were dried at 90 °C for more than 12 hours. First a masterbatch, containing 10 m% of the nanofillers was prepared, which then was diluted in a second extrusion-step to the desired concentrations of 2.5 and 5 m%, using a reduced screw speed of 40 rpm. Neat PA 11 was subjected to an identical processing history, serving as reference for the crystallization studies and accounting for possible processing-related changes of the molar mass. The extruded strands were cooled in a water bath, followed by granulation.

Instrumentation

Differential scanning calorimetry (DSC): Crystallization of PA 11 and its nanocomposites at low supercooling of the melt and at slow-cooling conditions was studied using a calibrated Mettler-Toledo heat-flux DSC 1 equipped with a Huber TC100 intracooler. The furnace was purged with nitrogen gas using a flow rate of 60 mL min^{-1}, in order to prevent sample degradation. Specimens with a mass about 5 mg were prepared from the extruded pellets and placed into small 20 µL aluminum pans. Isothermal crystallization experiments were performed at temperatures between 170–180 °C, with the crystallization temperature approached by cooling the relaxed melt from 220 °C at a rate of 50 K min^{-1}. The kinetics

of crystallization was then quantified by evaluation of the time of the crystallization-induced exothermic heat-flow rate peak. Non-isothermal crystallization experiments included cooling of the samples at rates between 2 and 50 K min^{-1}, and evaluation of peak-temperatures and enthalpies of crystallization. After completion of both isothermal and non-isothermal crystallization the specimens were re-melted and used for the next experiment, with absence of irreversible molecular changes assured by reproducibility tests.

Fast Scanning Calorimetry (FSC): The Mettler-Toledo Flash DSC 1 was used for analysis of isothermal and non-isothermal crystallization of PA 11 based nanocomposites at conditions which cannot realized using conventional DSC, that is, at rapid cooling and at low crystallization temperatures. The instrument was connected to a Huber TC100 intracooler to allow for fast cooling and subambient-temperature operation. The sample environment was purged with nitrogen gas at a flow rate of 40 mL min^{-1}, to avoid degradation and condensation. From the as-extruded pellets thin sections with a thickness of about 15 µm were prepared using a Slee rotary microtome. Then theses sections were reduced in their lateral size to about 100 µm using a stereomicroscope and scalpel. A thin layer of silicon oil was distributed on a conditioned and corrected chip sensor serving to improve the thermal contact between the specimen and the chip membrane. Isothermal crystallization experiments were performed to determine the peak-time of crystallization in the temperature range between 60 and 160 °C, if not stated otherwise. In these experiments the melt was cooled from 220 °C at a rate of 1000 K s^{-1} to the crystallization temperature, to record then the isothermal exothermic heat flow during a period of 5 s. Subsequently the sample was re-melted before analysis of crystallization at a different temperature. Non-isothermal crystallization experiments included melting of the sample at 220 °C followed by cooling at rates between 1 and 5000 K s^{-1}. The cooling scans were analyzed regarding the occurrence of crystallization peaks and determination of their peak temperature. The crystallinity was evaluated from the subsequently recorded heating scans.

Transmission electron microscopy (TEM): A Leica EM UC6 Ultramicrotome with cryo-attachment equipped was employed to cut ultrathin sections at –80 °C with a diamond knife. Samples with a thickness of 90 ± 10 nm were cut from injection molded tensile test bars molded at 50 °C. The specimens were placed on 300 mesh copper grids, and then inserted into a Zeiss TEM LEO 912 Omega, operated at 120 kV. The obtained images

show the structure/nanofiller dispersion in a plane perpendicular to the long dimension of the molding.

Scanning Electron Microscopy (SEM): SEM images of OMMT and sepiolite nanofillers, in order to gain information about the shape and dimensions as well as surface features, were taken with the help of a Zeiss Ultra Plus Gemini 55 FESEM at 60 kV. For sample preparation, all the samples were coated with carbon.

Polarized light Optical Microscopy (POM): POM was used to obtain information about the effect of presence of the sepiolite and OMMT nanofillers on the spherulitic superstructure of PA 11. Specimens with a thickness of 15 µm were cut from the extruded pellets using a Slee microtome, re-melted between Plano cover slips, and slowly crystallized on cooling at a rate of 1 K min^{-1}. The microstructure was then analyzed using a Motic BA410 optical microscope with the samples placed between crossed polarizers. Images were captured with a Moticam 2300 CCD camera.

Results and Discussion

Figure 1 shows the morphology/habit and dimensions of the plate-like OMMT (left) and needle-like sepiolite nanofillers (right) used in the present work, before melt-mixing with PA 11. The left SEM image shows isolated OMMT particles revealing that their lateral dimension and thickness are of the order of magnitude of 1 µm and around 30–50 nm, respectively. The sepiolite fibers exhibit a diameter of close to 50 nm and are distinctly longer than 1 µm; apparently the fibers form bundle-like aggregates.

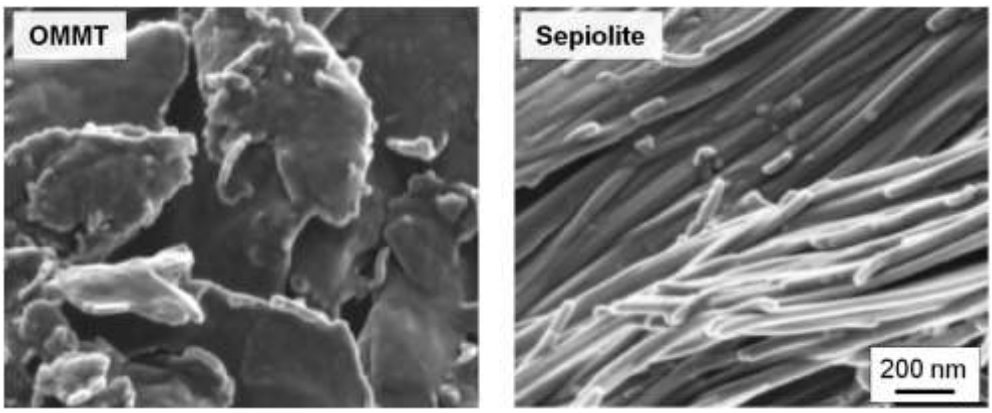

Figure 1: SEM images of OMMT (left) and sepiolite (right), taken before melt-compounding in PA 11. The scale bar holds for both images.

Figure 2 shows TEM images of PA 11 based nanocomposites containing OMMT (top row) and sepiolite (bottom row). The images at the left-hand and right-hand sides represent the structure of samples containing 2.5 and 5 m% nanofiller, respectively. To allow a direct comparison of the size of the nanofillers, the field of view is identical in all images, that is, the scale bar of 50 nm holds for all four pictures. The insets show typical features of the observed structure at a larger magnification.

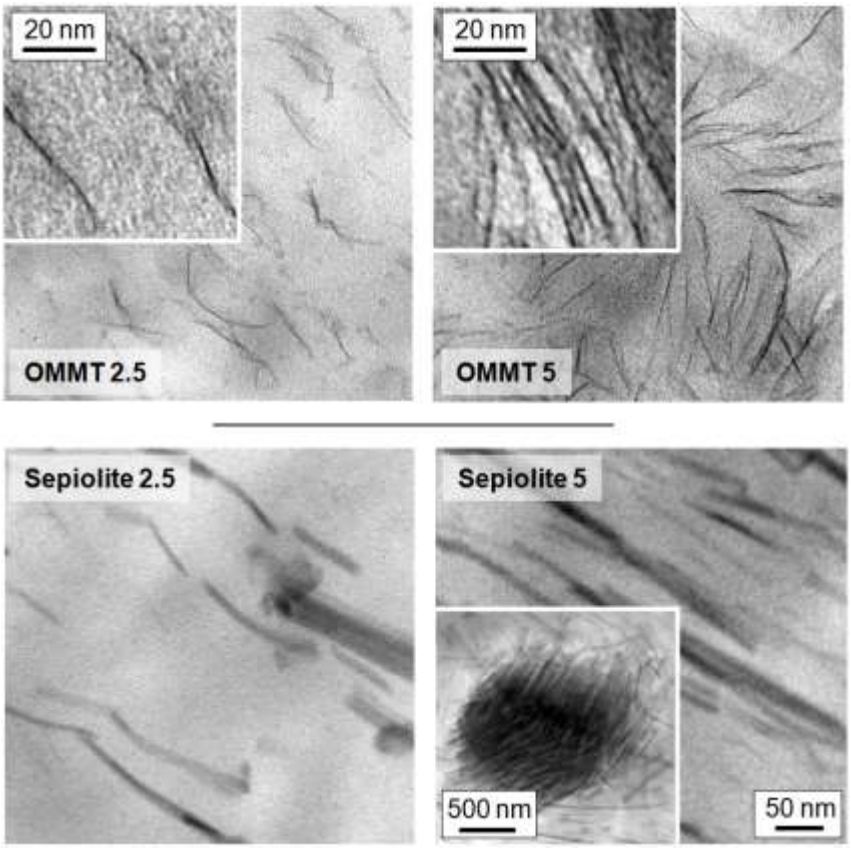

Figure 2: TEM images of PA 11 based nanocomposites containing OMMT (top row) and sepiolite (bottom row). The images at the left-hand and right-hand sides represent the structure of samples containing 2.5 and 5 m% nanofiller, respectively. The scale bar of 50 nm in the bottom right picture holds four all four images.

The images of the top row show well-dispersed edge-on viewed OMMT platelets with a lateral dimension of 50–100 nm and a thickness of few nm. In particular the inset in the top left image indicates that a high degree of intercalation and at least partially even complete exfoliation of the initially, that is, before melt-compounding, present galleries (see left image in Figure 1) was achieved with the selected processing/compounding route. It can be seen that the thickness of the clay particles is around 1–2 nm, which compares with a long period of 1.85 nm in the as-delivered OMMT powder [45], supporting our view of

presence of exfoliated sheets. Simultaneously, in particular in the sample containing 5 m% OMMT (top right image), there is occasionally observed incomplete dispersion/exfoliation of the OMMT nanofiller, which is recognized by still present stacks of individual clay layers, though with intercalated polymer (see inset).

The bottom two images of Figure 2 reveal presence of well-dispersed individual sepiolite fibers with a diameter between 10 and 50 nm, and length shorter than 1 µm. Obviously, extruder processing led to fracture of the initially much longer fibers (see right image in Figure 1). Similar as in case of the nanocomposite containing 5 m% OMMT, an increase of the concentration of the sepiolite fibers in the nanocomposite is connected with incomplete deagglomeration as is demonstrated with the inset in the bottom right image, showing a fiber cluster with a dimension close to 1 µm.

The non-isothermal crystallization behavior is explained with Figures 3 and 4. Figure 3 is a plot of temperatures of crystallization of PA 11 (gray squares) and its nanocomposites with 2.5 and 5 m% OMMT (blue triangles and stars) and 2.5 and 5 m% sepiolite (red circles and diamond symbols) as a function of the cooling rate. Data obtained on samples cooled at 0.83 K s^{-1} (50 K min^{-1}), or slower, were gained by DSC, otherwise FSC has been used. Regardless the specific differences between the various data sets of Figure 3, there is observed for all samples a decrease of the crystallization temperature with increasing rate of cooling the melt, being related to the kinetics of the crystallization process. For neat PA 11, the crystallization temperature on rather slow cooling at 0.033 K s^{-1} (2 K min^{-1}) is around 170 °C, however, decreases to values lower than 100 °C if the cooling rate is increased beyond 100 K s^{-1}. Simultaneously, at such fast cooling, there is detected mesophase formation at even lower temperatures close to 50 °C (light gray squares), which is caused by incomplete δ/α-crystal formation at higher temperature. Crystallization and mesophase formation are completely suppressed on cooling faster than 600 K s^{-1}, being in accord with data observed in an independent study.

Regarding the crystallization temperatures of the nanocomposites, several clear-cut facts are obtained from Figure 3. First of all, similar to prior studies on polyamide-based nanocomposites with OMMT, the effect of the presence of nanofiller on the crystallization temperature is rather negligible at slow-cooling conditions. The crystallization temperature increased by only few Kelvin in the DSC-cooling experiments. However, if the cooling

rate exceeds about 5 K s^{-1}, then the nucleating effect of the nanofillers becomes obvious since the crystallization-temperature difference between neat PA 11 and PA 11 nanocomposites is then distinctly increased. Furthermore there is observed with the data of Figure 3 that in case of both nanocomposite systems, PA 11/OMMT and PA 11/sepiolite, an increase of the nanofiller concentration beyond 2.5 m% is ineffective from the point-of-view of an attempted increase of the crystallization temperature. This behavior may be explained with the observed incomplete deagglomeration of sepiolite fibers and exfoliation of OMMT layers as were shown with right-hand side TEM images of Figure 2, ultimately reducing the nanofiller/polymer interfacial area which is important for the heterogeneous crystal nucleation process. Needless to say the distribution and dispersion of the nanofiller in the polymer matrix depends on the specific processing/melt-compounding route. In other words, variation of the nanocomposite-preparation scheme may lead to different results, though in this work a state-of-the art compounding technique was applied. Finally, the data of Figure 3 reveal that the crystal-nucleation efficiency of OMMT layers is superior of that of the sepiolite needles; in particular on cooling at rates faster than 100 K s^{-1} the different action of the sepiolite and OMMT nanofillers can be seen by the higher PA 11 crystallization temperature in presence of the latter.

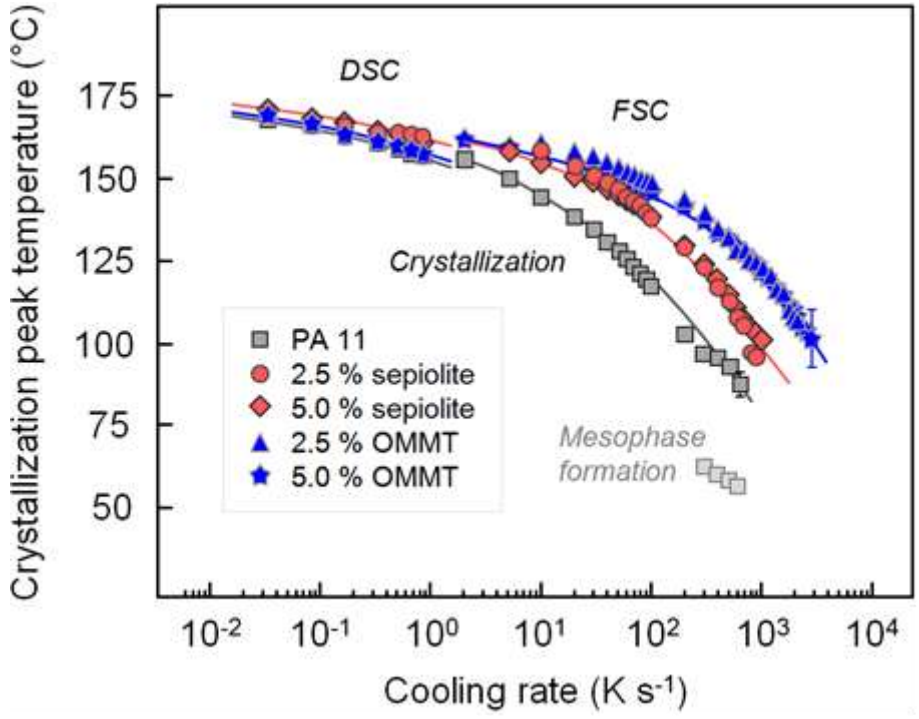

Figure 3: Crystallization-peak temperature of PA 11 (gray squares) and its nanocomposites with 2.5 and 5 m% OMMT (blue triangles and stars) and 2.5 and 5 m% sepiolite (red circles and diamond symbols) as a function of the cooling rate. Data of samples cooled at 0.83 K s^{-1} (50 K min^{-1}), or slower, were collected by DSC, otherwise FSC has been used.

In accord with the observation of increased crystallization temperatures of PA 11 in presence of sepiolite fibers and OMMT platelets, the cooling-rate range in which crystallization can occur is increased. While crystallization and mesophase formation in neat PA 11 only is observed on cooling slower than 600 K s^{-1}, in the nanocomposite with sepiolite and OMMT, the melt needs to be cooled faster than 1000 and 3000 K s^{-1} to below the glass transition temperature in order to prevent ordering, respectively.

Figure 4 shows the enthalpy of crystallization of PA 11 (gray squares) and its nanocomposites with 2.5 and 5 m% OMMT (blue triangles and stars) and 2.5 and 5 m% sepiolite (red circles and diamond symbols) as a function of the cooling rate. Since the mass of FSC samples, typically being around 100 ng, is difficult to determine precisely, enthalpies of crystallization from FSC experiments were estimated by scaling the obtained absolute transition enthalpies in order to fit the data obtained by DSC. The enthalpy of crystallization of neat PA 11 on slow cooling is about 50 J g^{-1}, which is equivalent to a crystallinity of around 26 % if a bulk enthalpy of crystallization of 189 J g^{-1} is used for its calculation. With increasing cooling rate there is first observed an only slight decrease of the crystallinity before it rapidly declines if the cooling rate exceeds about 100 K s^{-1}. Most striking regarding the data of Figure 4, however, is the observation of an increased enthalpy of crystallization/crystallinity of PA 11 in presence of the nanofillers, regardless the cooling rate. While on slow cooling the enthalpy of crystallization of neat PA 11 is 50 J g^{-1}, in the nanocomposites with sepiolite and OMMT the enthalpy of crystallization of PA 11 is around 55 and 62 J g^{-1}, respectively. In other words, there is observed a relative increase of the crystallinity of PA 11 by about 10 and 20 % in the nanocomposites, with the larger increase in the system containing OMMT being in qualitative agreement with higher crystallization temperature, compared to the nanocomposites containing sepiolite. Note that for the determination of the enthalpy of crystallization of the PA 11 matrix the reduced amount of polymer in the DSC samples containing nanofiller has been considered. Similar as in case of the crystallization temperatures, there is not detected an increase of the crystallinity when increasing the nanofiller content from 2.5 to 5 m%, presumably due to the deagglomeration/exfoliation reason as discussed above. Furthermore, and as it is emphasized with the vertical arrows, the data of Figure 4 illustrate again that the critical cooling rate above which crystallization is suppressed increases from 600 K s^{-1} in neat PA 11, to 1000–2000 and about 3000 K s^{-1} in the nanocomposites containing sepiolite and OMMT, respectively (see vertical arrows).

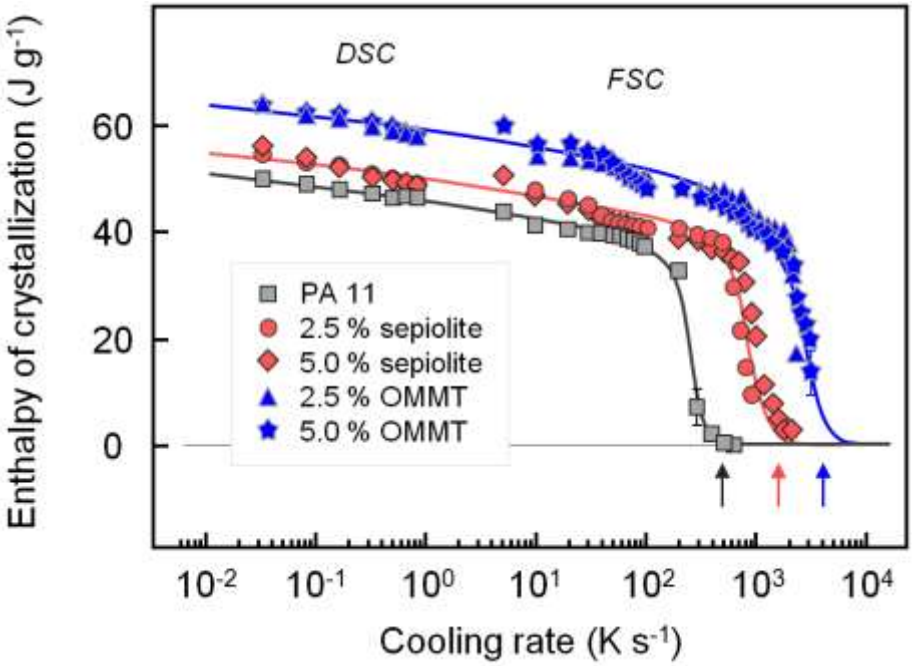

Figure 4: Enthalpy of crystallization of PA 11 (gray squares) and its nanocomposites with 2.5 and 5 m% OMMT (blue triangles and stars) and 2.5 and 5 m% sepiolite (red circles and diamond symbols) as a function of the cooling rate. Data of samples cooled at 0.83 K s^{-1} (50 K min^{-1}), or slower, were collected by DSC, otherwise FSC has been used. The vertical arrows indicate critical cooling rates above which crystallization is suppressed.

The nucleating effect of the nanofillers on the crystallization of the PA 11 matrix in the nanocomposites, as it was detected with the non-isothermal crystallization experiments discussed with Figures 3 and 4, is confirmed by isothermal analyses of the crystallization kinetics. Figure 5 is a plot of peak-times of crystallization of PA 11 (gray squares) and its nanocomposites with 2.5 and 5 m% OMMT (blue triangles and stars) and 2.5 and 5 m% sepiolite (red circles and diamond symbols) as a function of the crystallization temperature. With respect to the data points obtained on unmodified PA 11 (gray squares) it is observed that the peak-time of crystallization decreases with increasing supercooling due to increasing thermodynamic driving for the crystallization [50, 51], passes through a minimum at 110–120 °C and then begins to increase because of the decreasing mobility of chain segments. At high supercooling, at temperatures slightly below about 100 °C, there is then observed a rapid increase of the crystallization rate due to a change from heterogeneous nucleation, evident at high temperature, to homogeneous nucleation, prevailing at low temperature. Note that the change of the nucleation mechanism on variation of the supercooling of the melt has been investigated in an independent study [21, 22]. Most important in the context of the present work, however, is the observation of a decrease of the characteristic time of crystallization of PA 11 due to the presence of the

nanofillers. In case of the nanocomposites, data were only collected at temperatures higher than 130 and 150 °C for the systems containing sepiolite and OMMT, respectively, which is due to instrumental reasons since analysis of processes faster than about 10-100 milliseconds is impossible with the device used. This notwithstanding, the data of Figure 5 clearly reveal that the nucleating effect of the nanofillers on the crystallization of PA 11 increases with the supercooling of the melt, and also confirm the higher nucleation efficiency of the OMMT nanofiller compared to sepiolite; while for neat PA 11 the peak time of crystallization, which is close to the crystallization half-time, is around 1 s at 150 °C, in case of the nanocomposites with sepiolite and OMMT it is reduced to about 0.3 and less than 0.1 s, respectively, at identical temperature of crystallization. In other words, at 150 °C the crystallization rate of PA 11 in a nanocomposite with 2.5 m% OMMT is increased by more than one order of magnitude compared to neat PA 11.

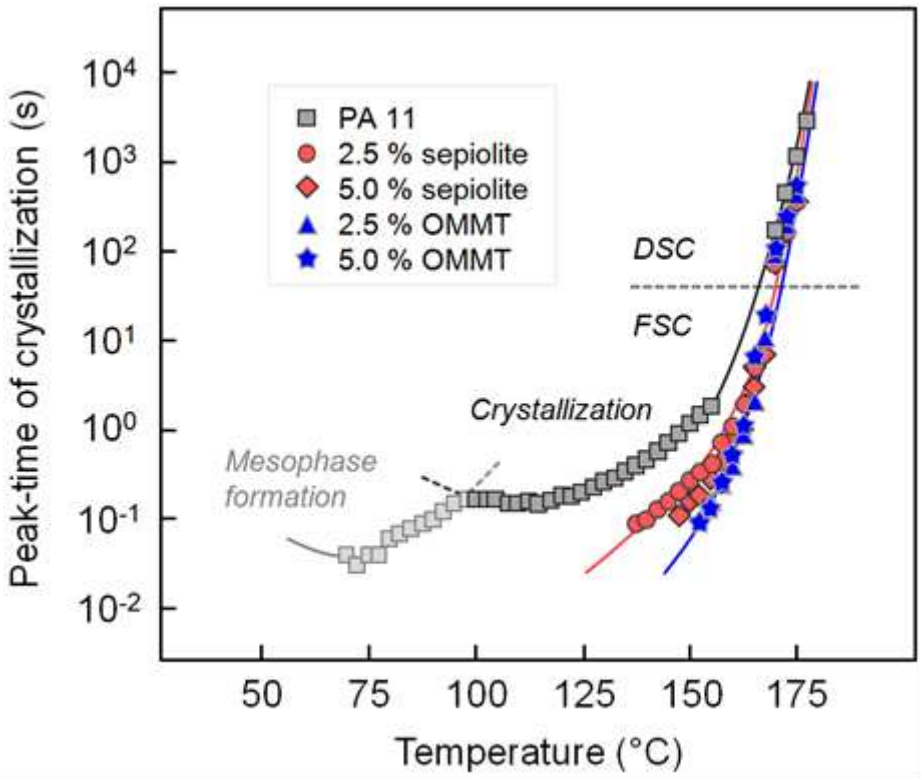

Figure 5: Peak-time of crystallization of PA 11 (gray squares) and its nanocomposites with 2.5 and 5 m% OMMT (blue triangles and stars) and 2.5 and 5 m% sepiolite (red circles and diamond symbols) as a function of the crystallization temperature. Data points referring to peak-times of crystallization longer than 50 s were collected by DSC, otherwise FSC has been used.

With the horizontal dashed line in Figure 5 is indicated the use of different instrumentation for obtaining information about the crystallization kinetics. Peak-times of crystallization longer than 50 s were measured by DSC, otherwise FSC was employed. The data reveal

that analysis of the kinetics of crystallization of PA 11 and its nanocomposites using DSC, that is, at rather low supercooling of the melt, provides only limited information about the nucleating effect of the nanofiller. Similar as in slow-cooling experiments, which enforced crystallization at low melt-supercooling (see Figure 3), negligible differences of the crystallization kinetics are detected by DSC, emphasizing the need to employ alternative analytical tools, such as the FSC, for identification of the nucleating effect of the nanofillers.

In both non-isothermal and isothermal crystallization experiments it has been found that the nucleating effect of the OMMT and sepiolite nanofillers on the crystallization of PA 11 levels out at rather low concentration of around 2.5 m%. This finding is illustrated and further quantified with the data plotted in Figure 6. With the bottom two data sets, associated with the left axis, are shown crystallization temperatures obtained on cooling at 100 K s^{-1}, and with the top two data sets, associated with the right axis, are shown crystallization peak-times at a temperature of 150 °C as a function of the OMMT (red, squares) and sepiolite (blue, circles) nanofiller concentration. It can be seen that for both nanofillers the crystallization temperature and characteristic crystallization time obviously are independent on the concentration if the loading is higher than 2.5 m%, confirming the consistency of the different experimental approaches to quantify the crystallization kinetics of PA 11 in nanocomposites. This holds also for the detection of a higher nucleation efficiency of the OMMT platelets in comparison to the sepiolite fibers; both, the increase of the crystallization temperature and decrease of the characteristic time of crystallization are larger for the OMMT nanofiller. Regarding the inefficiency of the nanofillers to further accelerate crystallization at loadings higher than 2.5 m%, incomplete dispersion/deagglomeration during processing is suggested as the cause for this behavior. This notwithstanding, the increase of the crystallization kinetics of PA 11 on nanofiller loading of 2.5 m% is considered remarkable, as the observed acceleration is of similar order of magnitude as it may be achieved when using classical nucleation agents [46, 47].

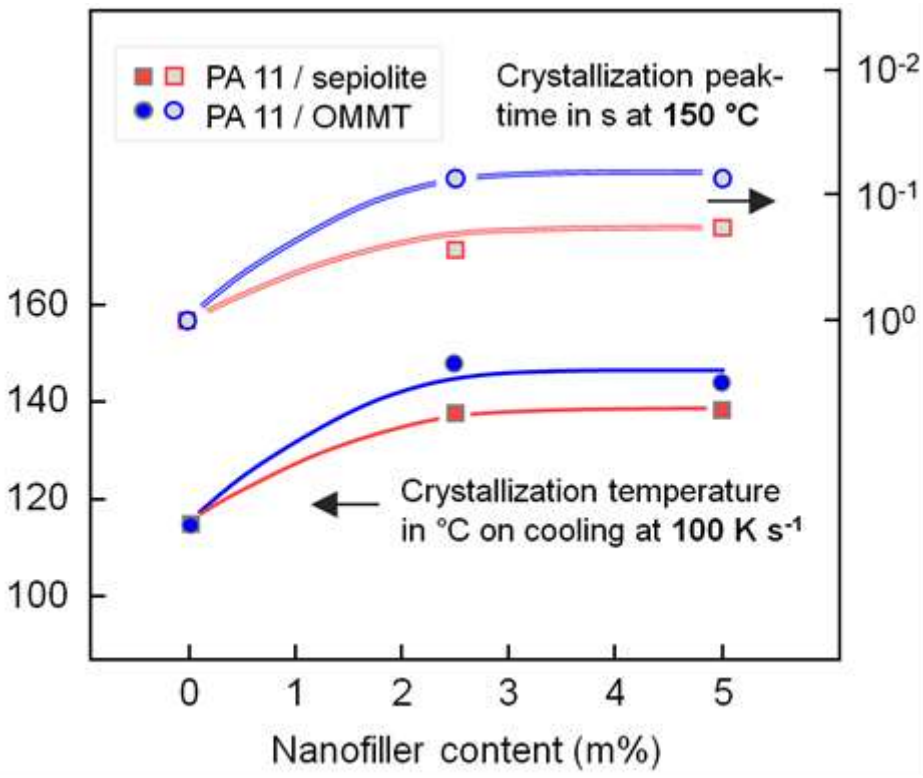

Figure 6: Crystallization temperature on cooling at 100 K s^{-1} (left axis, bottom two data sets) and peaks-time of crystallization at 150 °C (right axis, top two data sets) of PA 11 as a function of the content on OMMT (blue, circles) and sepiolite (red, squares).

The data of Figures 3–5 showed that melt-crystallization of PA 11 is accelerated in presence of the OMMT and sepiolite. It is assumed that these nanofillers support heterogeneous crystal nucleation at their surface. In other words, the observed increase of the overall crystallization rate in the nanocomposites, as it is detected with the increase of the crystallization temperature and decrease of crystallization time, is explained with an increase of the nucleation density compared to neat PA 11, but not by an increase of the crystal growth rate. The assumption of an increase of the nucleation density in nanocomposites is evidenced by analysis of the spherulitic superstructure using POM. The left, center, and right micrographs of Figure 7 were obtained on neat PA 11 and the PA 11 nanocomposites with 2.5 m% OMMT and sepiolite, respectively, with the specimens crystallized on slow cooling of the melt at a rate of 1 K min^{-1}. Qualitative inspection of the images shows that the micrometer scale structure of the nanocomposites is distinctly finer than the structure of neat PA 11. While in the left image obtained on unmodified PA 11 individual spherulites with a size of up to 10–20 µm can be identified, in case of the nanocomposites such detection of larger structural entities fails. Comparing the microstructures of the nanocomposites with OMMT (center) and sepiolite (right), it

appears that the addition of sepiolite leads to an even finer morphology than the addition of OMMT, despite the calorimetric data showed a higher nucleation efficiency in case of the latter nanofiller. The reason for this observation is not clear, and it may be speculated at this stage of research that despite a higher number of heterogeneous nuclei in the system containing sepiolite the overall crystallization rate is reduced compared to the system with OMT, for example by mobility constraints [35].

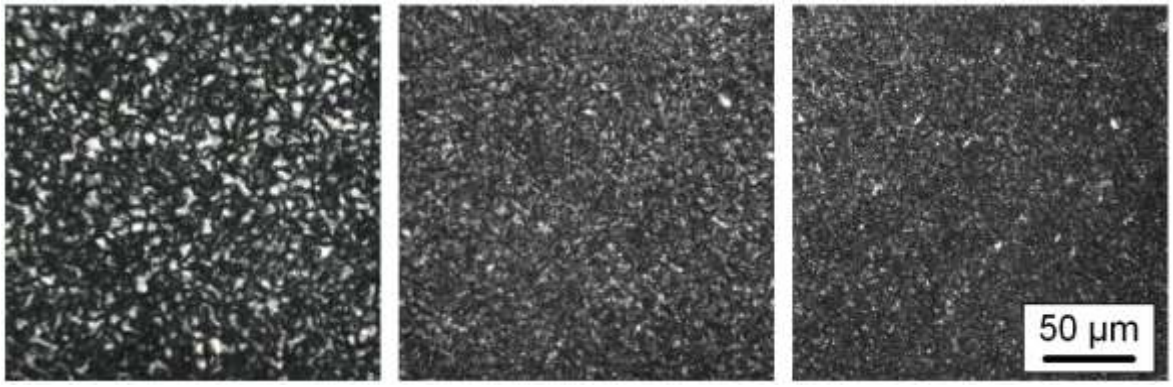

Figure 7: POM images obtained on neat PA 11 (left) and nanocomposites of PA 11 with 2.5 m% OMMT (center) and 2.5 m% sepiolite (right). The samples were prepared by slow cooling of the melt at a rate of 1 K min^{-1}.

Conclusions

The crystallization kinetics of PA 11 in presence of sepiolite and OMMT nanofillers has been studied in a wide range of temperatures and cooling rates using DSC and FSC. There is observed negligible effect of the nanofillers on the crystallization temperature of PA 11 at low cooling rates as well as on isothermal crystallization at low supercooling of the melt. At rapid cooling conditions, however, a distinct nucleating effect of the nanofillers is detected by the observation of increased crystallization temperatures. Simultaneously, the critical cooling rate to suppress crystallization increases from 600 K s^{-1} in case of neat PA 11 to about 1000 and 3000 K s^{-1} in the nanocomposites containing sepiolite and OMMT, respectively. This observation suggests implications on structure formation in processing, as for example injection molding may be connected with cooling the melt at such high rates. In agreement with the non-isothermal experiments which revealed a nucleating effect of the nanofillers in particular at high cooling rates, enforcing crystallization at low temperature, in isothermal crystallization experiments there is detected a large decrease of the crystallization time of PA 11 in the nanocomposites at rather high supercooling of the melt.

It is suggested that the nanofillers support heterogeneous crystal nucleation at their surfaces with the observed increase of the overall crystallization rate then being explained with an increase of the nucleation density compared to neat PA 11. This assumption seems justified with the observed change of the spherulitic superstructure which shows that the micrometer-scale structure of the nanocomposites is distinctly finer than the structure of neat PA 11. Apparently, the addition of sepiolite leads to an even finer morphology than the addition of OMMT, despite higher nucleation efficiency is seen for the latter nanofiller. It may be speculated that despite a higher number of heterogeneous nucleation sites in the system containing sepiolite, the overall crystallization rate is reduced for example by segment-mobility constraints. This notion is supported by the observation that nanofiller loadings greater than 2.5 m% are not associated with a further acceleration of the crystallization rate. This can be caused by incomplete deagglomeration of the initial nanoparticle clusters, as it was demonstrated with TEM analyses, but also by presence of large rigid amorphous fraction of PA 11, hindering the crystal growth.

Acknowledgments

Financial support by the Deutsche Forschungsgemeinschaft (DFG) (Grant AN 212/18) is gratefully acknowledged.

References

[1] Rilsan Product Information, available at www.arkema.com.

[2] Brazel CS, Rosen SL. Fundamental principles of polymeric materials. Wiley, 2012.

[3] Mollova A, Androsch R, Mileva D, Schick C, Benhamida A. Effect of supercooling on crystallization of polyamide 11. Macromolecules 2013;46:828–835.

[4] Kargin VA, Sogolova TI, Rapoport N Ya, Kurbanova II. Effect of artificial nucleating agents on polymers structure and properties. J Polym Sci, Polym Symp 1967;16:1609–1617.

[5] Paul DR, Robeson LM. Polymer nanotechnology: Nanocomposites. Polymer 2008;49:3187–3204; Fornes TD, Paul DR. Modeling properties of nylon 6/clay nanocomposites using composite theories. Polymer 2003;44:4993–5013.

[6] Mathias LJ, Powell DG, Autran JP, Porter RS. ^{15}N NMR characterization of multiple crystal forms and phase transitions in polyundecanamide (Nylon 11). Macromolecules 1990;23:963–967.

[7] Nair SS, Ramesh, C Tashiro K. Polymorphism in Nylon 11: Characterization using HTWAXS and HTFTIR. Macromol Symp 2006;242:216–226.

[8] Newman BA, Sham TP, Pae KD. A high-pressure x-ray study of Nylon 11. J Appl Phys 1977;48:4092–4098.

[9] Schmidt GF, Stuart HA. Gitterstrukturen mit räumlichen Wasserstoffbrückensystemen und Gitterumwandlungen bei Polyamiden. Zeitschr Naturforschung (A) 1958;13:222–225.

[10] Gogolewski S. Effect of annealing on thermal properties and crystalline structure of polyamides. Nylon 11 (polyundecaneamide). Coll Polym Sci 1979;257:811–819.

[11] Zhang Q, Mo Z, Zhang H, Liu S, Cheng SZD. Crystal transitions of Nylon 11 under drawing and annealing. Polymer 2001;42:5543–5547.

[12] Brill R. Beziehungen zwischen Wasserstoffbindung und einigen Eigenschaften von Polyamiden. Makromol Chemie 1956;18:294–309.

[13] Zhang Q, Mo Z, Liu S, Zhang H. Influence of annealing on structure of Nylon 11. Macromolecules 2000;33:5999–6005.

[14] Wunderlich B. The athas database on heat capacities of polymers see on WWW URL: http://www.springermaterials.com/docs/athas.html, Pure and Applied Chemistry 1995;67(6):1019–1026.

[15] Inoue M. Studies on crystallization of high polymers by differential thermal analysis. J Polym Sci, Part A 1963;1:2697–2709.

[16] Magill JH. Formation of spherulites in polyamides. IV. Even-odd polyamides and poly(ω-aminocarboxylic acids). J Polym Sci, Part A-2 1969;7:123–142.

[17] Androsch R, Schick C. Crystal nucleation of polymers at high supercooling of the melt. Adv Polym Sci, in print, DOI: 10.1007/12_2015_325.

[18] Xu W, Ge M, He P. Nonisothermal crystallization kinetics of polypropylene/montmorillonite nanocomposites. J Polym Sci, Polym Phys 2002;40:408–414.

[19] Maiti P, Nam PH, Okamoto M. Influence of crystallization on intercalation, morphology, and mechanical properties of polypropylene/clay nanocomposites. Macromolecules 2002;35:2042–2049.

[20] Yuan Q, Awate S, Misra RDK. Nonisothermal crystallization behavior of polypropylene-clay nanocomposites. Eur Polym J 2006;42:1994–2003.

[21] Xu W, Ge M, He P. Nonisothermal crystallization kinetics of polyoxymethylene/montmorillonite nanocomposite. J Appl Polym Sci 2001;82:2281–2259.

[22] Wang Y, Gao J, Ma Y, Agarwal US. Study on mechanical properties, thermal stability and crystallization behavior of PET/MMT nanocomposites. Composites: Part B: Engineering 2006;37:399–407.

[23] Wu D, Zhou C, Fan X, Mao D, Bian Z. Nonisothermal crystallization kinetics of poly(butylene terephthalate)/montmorillonite nanocomposites. J Appl Polym Sci 2006;99:3257–3265.

[24] Mollova A, Kolesov I, Androsch R, Labuschagne J, Focke W, Funari SS. Crystallization of nanocomposites of an isotactic random butene-1/ethylene copolymer and layered double hydroxide. Polym Bull 2013;70:3115–3128.

[25] Liu X, Wu Q, Berglund LA. Polymorphism in polyamide 66/clay nanocomposites. Polymer 2002;43:4967–4972.

[26] Wu Z, Zhou C, Zhu N. The nucleating effect of montmorillonite on crystallization of nylon 1212/montmorillonite nanocomposites. Polym Testing 2002;21:479–483.

[27] Wu Q, Liu X, Berglund A. An unusual crystallization behavior in polyamide 6/montmorillonite nanocomposites. Macromol Rap Comm 2001;22:1438–1440; Liu X, Wu Q, Berglund LA. Investigation on unusual crystallization behavior in polyamide 6/montmorillonite nanocomposites. Macromol Mat Eng 2002;287:515–522; Liu X, Wu Q. Non-isothermal crystallization behaviors of polyamide 6/clay nanocomposites. Eur Polym J 2002;38:1383–1389.

[28] Lincoln DM, Vaia RA. Isothermal crystallization of nylon-6/montmorillonite nanocomposites. Macromolecules 2004;37:4554–4561; Lincoln DM, Vaia RA,Wang Zg, Hsiao BS, Krishnamoorti R. Temperature dependence of polymer crystalline morphology in nylon 6/montmorillonite nanocomposites. Polymer 2001;42:9975–9985.

[29] Tjong SC, Bao SP. Preparation and nonisothermal crystallization behavior of polyamide 6/montmorillonite nanocomposites. J Polym Sci, Polym Phys 2004;42:2878–2891.

[30] Liu L, Qi Z, Zhu X. Studies on Nylon 6/clay nanocomposites by melt-intercalation process. J Appl Polym Sci 1999;71:1133–1138.

[31] Fornes TD, Paul DR. Crystallization behavior of Nylon 6 nanocomposites. Polymer 2003;44:3945–3961.

[32] Mileva D, Monami A, Cavallo D, Alfonso GC, Portale G, Androsch R. Crystallization of a polyamide 6/montmorillonite nanocomposite at rapid cooling. Macromol Mat Eng 2013;298:938–943.

[33] Ishisue T, Okamoto M, Tashiro K. Real-time investigation of crystallization in nylon 6-clay nano-composite probed by infrared spectroscopy. Polymer 2010;51:5585–5591; Katoh Y, Okamoto M. Crystallization controlled by layered silicates in nylon 6-clay nano-composites. Polymer 2009;50:4718–4726.

[34] Mathias LJ, Davis RD, Jarrett WL. Observation of α and γ crystal forms and amorphous regions on Nylon 6-clay nanocomposites using solid-state ^{15}N nuclear magnetic resonance. Macromolecules 1999;32:7958–7960.

[35] Wurm A, Ismail M, Kretschmar B, Pospiech D, Schick C. Retarded crystallization in polyamide/layered silicates nanocomposites caused by an immobilized interphase. Macromolecules 2010;43:1480–1487.

[36] Homminga DS, Goderis B, Mathot VBF, Groeninckx G. Crystallization behavior of polymer/montmorillonite nanocomposites. Part III. Polyamide-6/montmorillonite nanocomposites, influence of matrix molecular weight, and of montmorillonite type and concentration. Polymer 2006;47:1630–1639.

[37] Zhang Q, Yu M, Fu Q. Crystal morphology and crystallization kinetics of polyamide-11/clay nanocomposites. Polym Int 2004;53:1941–1949.

[38] Fornes TD, Paul DR. Structure and properties of nanocomposites based on nylon 11 and nylon 12 compared with those based on nylon 6. Macromolecules 2004;37:7698–7709.

[39] Liu T, Lim KP, Tjiu WC, Pramoda KP, Chen ZK. Preparation and characterization of nylon 11/organoclay nanocomposites. Polymer 2003;44:3529–3535.

[40] Halim KAA, Farrell JB, Kennedy JE. Preparation and characterization of polyamide 11/montmorillonite (MMT) nanocomposites for use in angioplasty balloon application. Mat Chem Phys 2013;143:336–348.

[41] Kolesov I, Androsch R, Mileva D, Lebek W, Benhamida A, Kaci M, Focke W. Crystallization of polyamide 11/organo-modified montmorillonite nanocomposite at rapid cooling. Coll Polym Sci 2013;291:2541–2549.

[42] Xie S, Zhang S, Wang F, Yang M, Séguéla R, Levebre JM. Preparation, structure and thermomechanical properties of nylon-6 nanocomposites with lamella-type and fiber-type sepiolite. Comp Sci Tech 2007;67:2334–2341.

[43] Bilotti E, Zhang R, Deng H, Quero F, Fischer HR, Peijs T. Sepiolite needle-like clay for PA6 nanocomposites: An alternative to layered silicates? Comp Sci Tech 2009;69:2587–595.

[44] Fukushima K, Tabuani D, Camino G. Nanocomposites of PLA and PCL based on montmorillonite and sepiolite. Mater Sci Eng 2009;C29:1433–1441.

[45] Cloisite® 30B, Product data sheet.

[46] Androsch R, Monami A, Kucera J. Effect of an alpha-phase nucleating agent on the crystallization kinetics of a propylene/ethylene random copolymer at largely different supercooling. J Crystal Growth 2014;408:91–96.

[47] Mollova A, Androsch R, Mileva D, Gahleitner M, Funari SS. Crystallization of isotactic polypropylene containing beta-phase nucleating agent at rapid cooling. Eur Polym J 2013;49:1057–1065.